Electronic Supplementary Material (ESI) for Journal of Materials Chemistry A.

Supplemental Information

Atomic-Confined-Space Separator for High Performance Lithium-Sulfur Batteries

Junya Cui‡[a], Zhenhua Li‡[a], Jianbo Li[a], Sai Li[b], Jun Liu[b], Mingfei Shao*[a] and Min Wei[a]

[a]State Key Laboratory of Chemical Resource Engineering, Beijing University of Chemical Technology, Beijing 100029, China

[b]Key Laboratory of Beijing City on Preparation and Processing of Novel Polymer Materials, Beijing University of Chemical Technology, Beijing 100029, China

‡These authors contribute equally to this work.

**Corresponding authors. E-mail addresses:* shaomf@mail.buct.edu.cn

1. Experimental Procedures

1.1 Synthesis of single MgAl-LDH nanosheet

1.1.1 Preparation of MgAl(CO_3^{2-})-LDH nanoplates

The sample of MgAl(CO_3^{2-})-LDH with well-defined hexagonal morphology was prepared *via* a homogeneous coprecipitation method. Typically, $Mg(NO_3)_2 \cdot 6H_2O$ (0.2 M), $Al(NO_3)_3 \cdot 9H_2O$ (0.1 M) and urea (1 M) were dissolved in 100 mL of deionized water. Then, the mixed solution was transferred into an autoclave and heated at 110 °C for 24 h. The resulting LDH were separated by centrifugation, washed three times with ethanol and deionized water, and finally dried in air under room temperature.

1.1.2 Preparation of MgAl(NO_3^-)-LDH nanoplates

The MgAl(NO_3^-)-LDH was prepared *via* a salt-acid exchange method. Typically, MgAl(CO_3^{2-})-LDH platelets (1.0 g) were added into an aqueous salt-acid solution (1 L) containing HNO_3 (0.0045 mol) and $NaNO_3$ (1.5 mol) in a three-neck flask. The suspension was stirred continuously at room temperature under N_2 flow for 24 h. The resulting MgAl(NO_3^-)-LDH platelets were centrifuged and washed with degassed water and absolute ethanol for three times.

1.1.3 Preparation of single-layer MgAl-LDH nanosheets

The single-layer MgAl-LDH colloidal suspension was obtained by dispersing 0.1 g of MgAl(NO_3^-)-LDH platelets in 100 mL formamide and stirring for 48 h.

1.2 Preparation of GO nanosheets

GO nanosheets were prepared using a modified Hummer's method. Typically, 0.5 g of graphite powder was dispersed in 11.5 mL of concentrated H_2SO_4 (98%) under 0 °C, followed by adding 1.5 g of $KMnO_4$ and keeping the temperature below 20 °C. The mixture was stirred at 35 °C for 2 h which was terminated by 90 mL of deionized water. Subsequently, 1 mL of 30% H_2O_2 was added to the solution and the color was changed to bright yellow. The mixture was washed with 10% HCl (125 mL) to remove residual metal ions and then washed with deionized water until the solution became neutral. Finally, the product was sonicated for 10 h and then centrifuged to remove the precipitate to obtain exfoliated GO solution.

1.3 Preparation of (LDH/GO)$_n$ ultrathin film (UTF) modified PP separator

1.3.1 Modifying polydopamine (PDA) on PP separator

The commercial PP separator (Celgard 2325) was modified by PDA to get negative charged surface. In this process, dopamine (80 mg) was added into 100 mL Tris-HCl buffer solution (pH= 8). Then, the PP separator was floated on the surface of above PDA solution under room temperature for 6 h to get single side modification.

1.3.2 Assembly of (LDH/GO)$_n$ UTF

The atom-thick (LDH/GO)$_n$ film was fabricated by layer-by-layer (LBL) assembly of MgAl-LDH nanosheets and graphene oxide nanosheets (GO NSs; prepared by a modified Hummers method). Typically, the side of the PP separator with the PDA modification was floated on the surface of MgAl-LDH colloidal suspension (PDA-modified side faces the solution and the unmodified side faces the air) for 10 min to adsorb positively charged LDH NSs under the driven of electrostatic force, followed by deionized water washing and nitrogen drying. Then, the separator was further attached to the surface of the GO colloidal suspension for 10 min to assemble negatively charged GO NSs, followed by deionized water washing and nitrogen drying. The cycle was repeated to reach the desired number of LDH/GO films. The prepared separator was slightly reduced in 0.2 g L^{-1} $NaBH_4$ solution for 2 minutes to realize the reduction of GO on the surface layer and then to improve the conductivity.

1.4 Preparation of sulfur cathode and polysulfide permeation test

1.4.1 Preparation of sulfur cathode

The sulfur cathode was prepared by casting a slurry that contains active material, super P and water soluble polymer *n*-lauryl acrylate (LA, 5%; Chengdu, China) in a mass ratio of 7:2:1

on copper foil. The active materials was prepared by mixing super P and sulfur powder with mass ratio of 7:3 by shaker-milling. Then, the mixture was sealed in a weighing bottle and heated at 155 °C for 6 h to incorporate sulfur into the micropore of super P. The sulfur content was approximately 75 wt% which was measured by thermogravimetric analysis (TGA).

1.4.2 Preparation of Li_2S_6 solution and the polysulfide permeation test

Li_2S_6 solution was prepared by mixing the lithium sulfide and sulfur in a molar ratio of 1:5 in DME/DOL solution (DOL:1,3-dioxolane, DME:1,2-dimethoxyethane; 1:1 volume ratio). The Li_2S_6 permeation test was performed in an H-type electrolytic cell, among which the Li_2S_6 solution and DME/DOL solution were added on both sides of the cell with different separators.

1.5 Characterization

The UV-Vis absorption spectra were measured on a Shimadzu UV-2501PC spectrophotometer. X-ray diffraction (XRD) data was obtained in a Shimadzu XRD-6000 power X-ray diffractometer using Cu Kα radiation (0.154 nm) at 40 kV, 30 mA,and scanning rate of 1° min^{-1}. Raman spectra were measured on Raman microspectrometer (Renishaw, inVia-Reflex, 532 nm) with 532 nm of excitation by using a confocal. The thickness and surface topography of the $(LDH/GO)_n$ were examined by atomic force microscope (AFM, Veeco, NanoScope IIIa), the $(LDH/GO)_n$ film was assembled on the quartz sheet and scratch a trace with a fine scalpel. The morphology was measured on a Zeiss SUPRA55 scanning electron microscope (SEM), which combine with energy dispersive X-ray spectroscopy (EDS). The Fourier transform infrared (FT-IR) spectra was recorded by a Vector 22 (Bruker) spectrophotometer using the KBr pellet technique in the range of 4000~400 cm^{-1} with 2 cm^{-1} resolution.

1.6 Electrochemical measurements

The CR2032 coin-type cells were assembled in an argon-filled glove box by using Li foils as anode and sulfur as cathode. The mass loading of S is 1.2 mg cm^{-2} or 4.0 mg cm^{-2}. The electrolyte was prepared by dissolving 1 M lithium trifluoromethanesulfonyl (LiTFSI) and 1 wt% $LiNO_3$ in DME/DOL solution. The amount of the electrolyte was 40 μL mg^{-1} of S. The galvanostatic charge-discharge curves were conducted on CT2001A cell test instrument (LAND Electronic Co. Ltd) with the voltage window of 1.7–2.8 V (versus Li^+/Li) under room temperature. The cyclic voltammogram (scan rate: 0.05-1 mV s^{-1}) and electrochemical impedance spectroscopy (EIS) (frequency range: 200 kHz-10 mHz) were performed with a CHI660E electrochemical workstation (Shanghai Chenhua Instrument Co, China).

Li-ion diffusion coefficient was calculated by the Randles-Sevcik equation based on the cyclic voltammetry (CV) curves under various scan rates from 0.1 to 0.5 mV s^{-1}:

$$I_p = 2.69 \times 10^5 n^{3/2} A D_{Li^+}^{1/2} C_{Li^+} v^{1/2}$$

where I_p is the peak current, *n* is the number of electrons transferred in the reaction (*n*=2 for Li-S batteries), A is the electrode area, D_{Li^+} is the Li-ion diffusion coefficient, C_{Li^+} is the change in the concentration of Li-ion, and v refers to the scan rate. The set-up for CV tests are as follows: Upper vertex potential (V): 3.000, Lower vertex potential (V): 1.500, Stop potential (V): 2.950, Number of stop crossings: 10, Step potential (V): 0.00500.

1.7 Preparation of Li–S prototype cell for operando Raman spectroscopy:

A disc cell with transparent quartz window was prepared with cathodes, PP separator/$(LDH/GO)_{20}$ separator and lithium foils, and the lithium foil with a diameter of 15 mm had a 5 mm central hole. The cathode and electrolyte are the same as other test cells. The cell was connected with a CHI660E electrochemical workstation (Shanghai Chenhua Instrument Co., China) for characterization of the electrochemical performance. Raman spectra were obtained by aligning the laser with the circular holes in the cathodes and lithium foils, through the quartz window.

1.8 Computational details

1.8.1 Model construction

Herein, we select the coarse-grained molecular dynamics simulation (CGMDS) to give a further insight into the diffusion of the two electrolyte particles on LDH/GO ultrathin film. The model of LDH/GO are built with a periodic border box which can reduce the amount of calculations of supercomputers. We use beads of different diameters to represent different materials in realistic. According to the mapping process, the beads with a diameter of 1σ correspond to Li ions and the beads with a diameter of 2σ represent the sulfur. Furthermore, four layers composed by beads are constructed to represent the atom-thick film that assembled by layered double hydroxide nanosheets and graphene oxide nanosheets and the four layers are fixed during the entire simulation. By giving the initial velocity of the two particles (Li and S), the two different types of beads do Brownian motion in space.

1.8.2 Computational details

The non-bonded interaction between all beads, including Li metal anode, sulfur cathode and layers, are described by the truncated and shifted Lennard-Jones (LJ) potential:

$$U(r)=\begin{cases}4\varepsilon\left[\left(\frac{\sigma}{r-\Delta}\right)^{12}-\left(\frac{\sigma}{r-\Delta}\right)^{6}\right]+C & r<r_{cutoff}+\Delta\\ 0 & r\geq r_{cutoff}+\Delta\end{cases}$$

Where the LJ interaction is cut off at the distance $r=2.5\sigma$, σ defines the length scale and ε is the pair interaction energy parameter. Δ takes into account the effect of the excluded volume of the different interaction sites. And C is a constant, which guarantees that the potential energy is continuous at the cutoff distance. Therefore, the actual cutoff distance is the sum of r_{cutoff} and Δ. The LJ potential was cut off at different distances to model the attractive or repulsive interaction. In order to match the interaction with the actual substance, we set all the non-bonded interaction between simulation model beads as the repulsive interaction.

2. Supplementary Figures and Tables

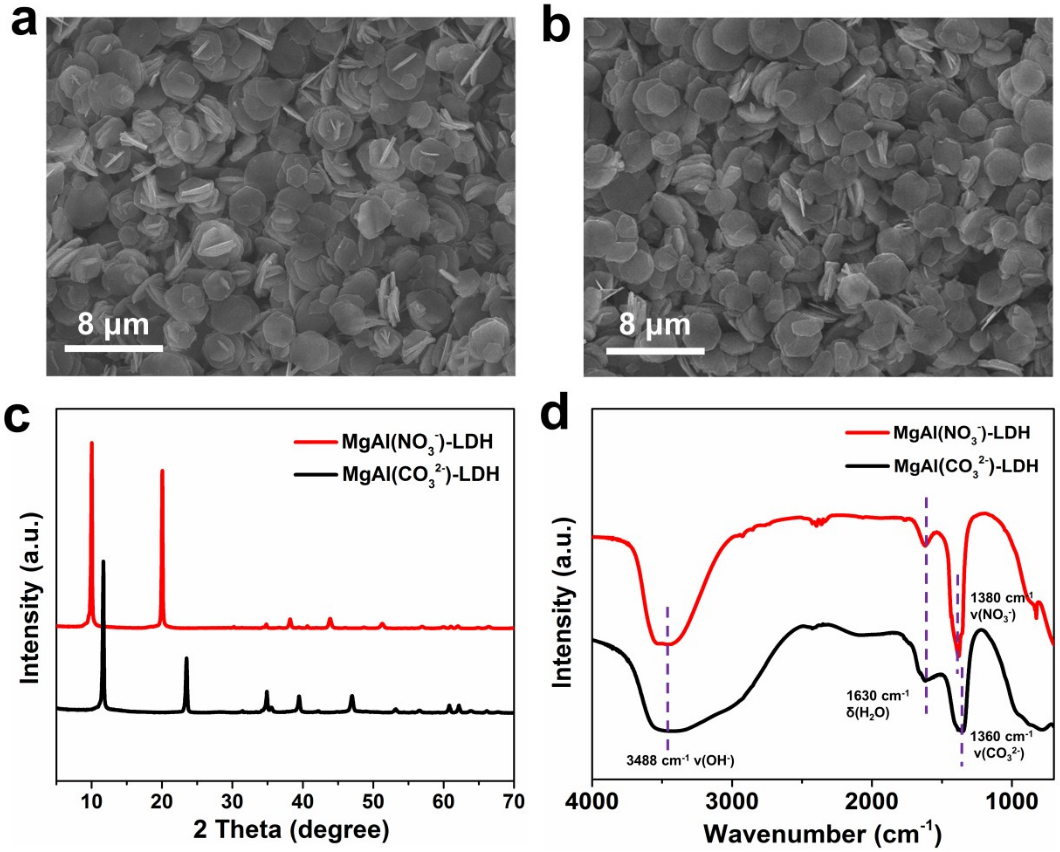

Figure S1. SEM images of (a) MgAl (CO_3^{2-})-LDH (b) MgAl (NO_3^-)-LDH. (c) XRD patterns and (d) FTIR spectra of MgAl (CO_3^{2-})-LDH and MgAl (NO_3^-)-LDH.

The scanning electron microscope (SEM) images in Figure S1a and S1b show that the hexagonal morphology of LDHs were well maintained while the interlayer anions is changed. This is confirmed by XRD pattern. As shown in Figure S1c, the typical (003) diffraction peak of MgAl (CO_3^{2-})-LDH is shifted from 11.5° to 10.1° after NO_3^- intercalation, which expands the interlayer distance and weakens the interaction between the LDH layers. Moreover, the FTIR spectra also confirm the change of interlayer anions from CO_3^{2-} to NO_3^-.

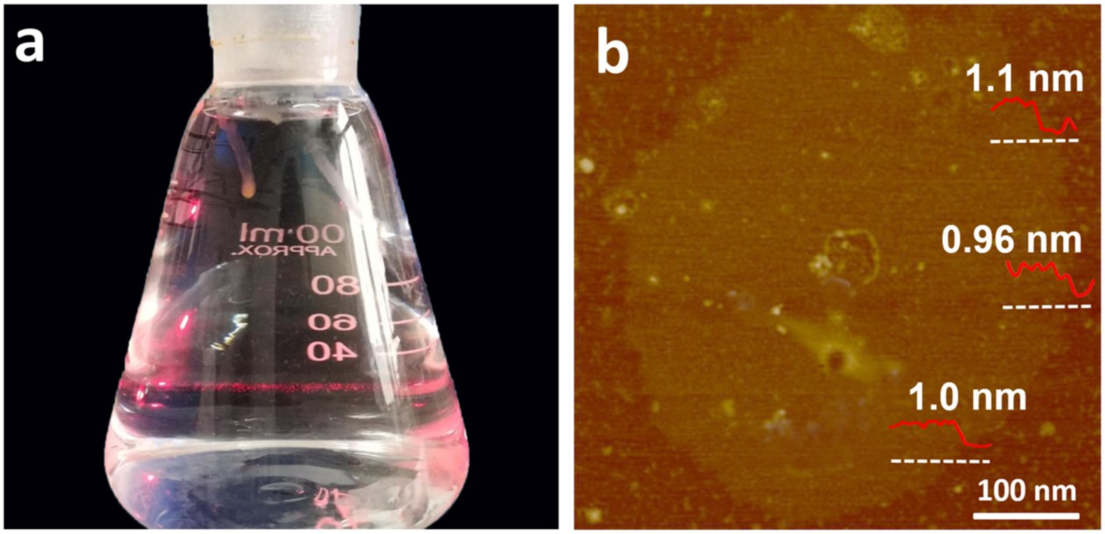

Figure S2. Photograph demonstration for the MgAl-LDH colloidal suspension. (b) The AFM image of the exfoliated MgAl-LDH nanosheets.

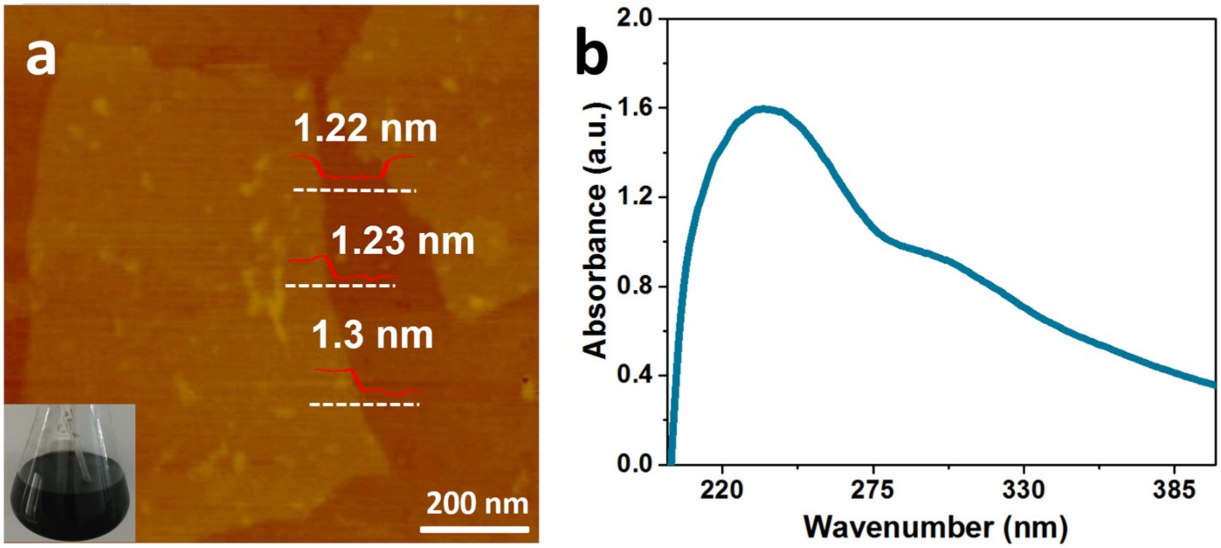

Figure S3. (a) The AFM image of the GO nanosheets (insert: photograph demonstration for the GO colloidal suspension). (b) UV-Vis absorption spectra of GO solution.

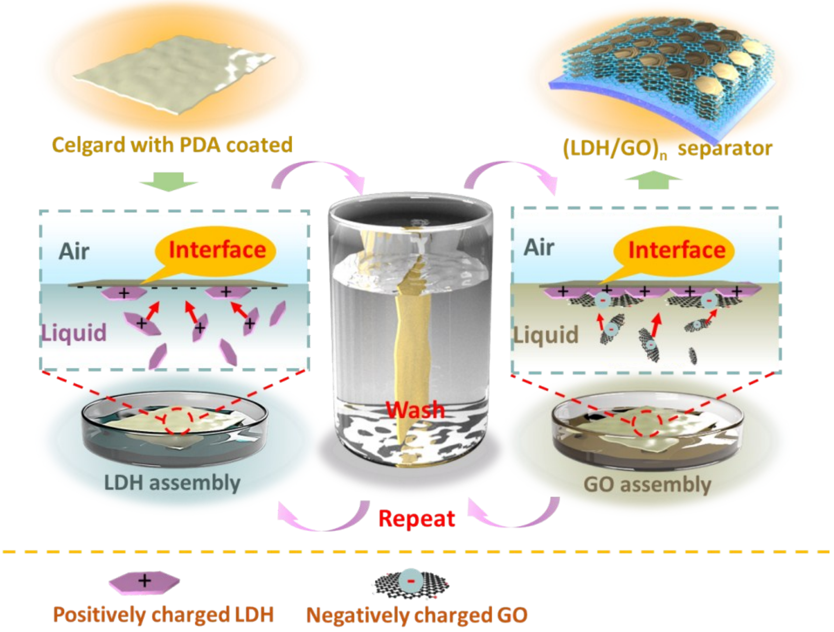

Figure S4. Schematic illustration for the LBL assembly process of (LDH/GO)$_n$ UTF on single side of PP separator.

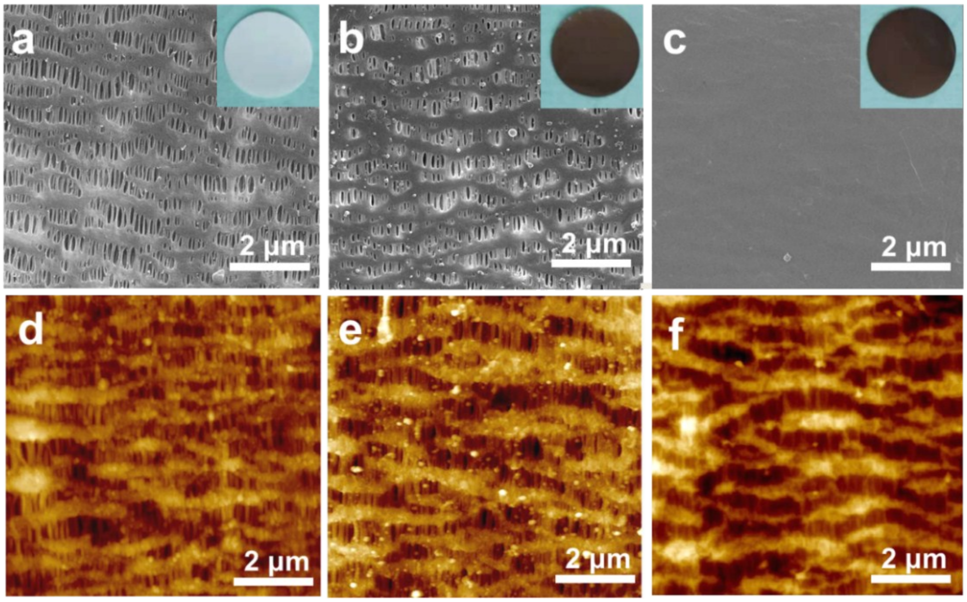

Figure S5. SEM images of (a) PP separator, (b) PDA/PP separator and (c) (LDH/GO)$_{20}$-PP separator. (d-f) the corresponding AFM images of the PP, PDA/PP and (LDH/GO)$_{20}$-PP separator (the surface roughness: R_a(PP)= 21.5 nm, R_a(PAD/PP)= 21.4 nm, R_a(LDH/GO)= 14.5 nm).

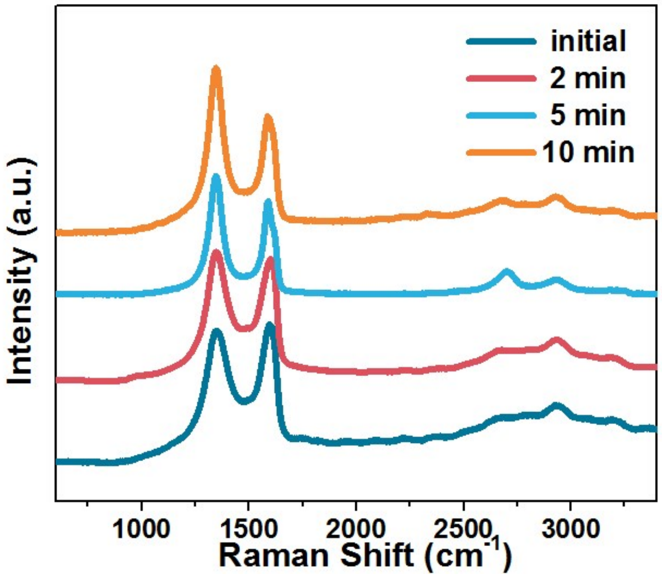

Figure S6. Raman spectra of (LDH/GO)$_{20}$-PP separator at different reduction times.

It can be seen that the intensity of the D peak gradually increased with the increase of reduction time, indicating that the reduction degree of graphene is gradually deepened.

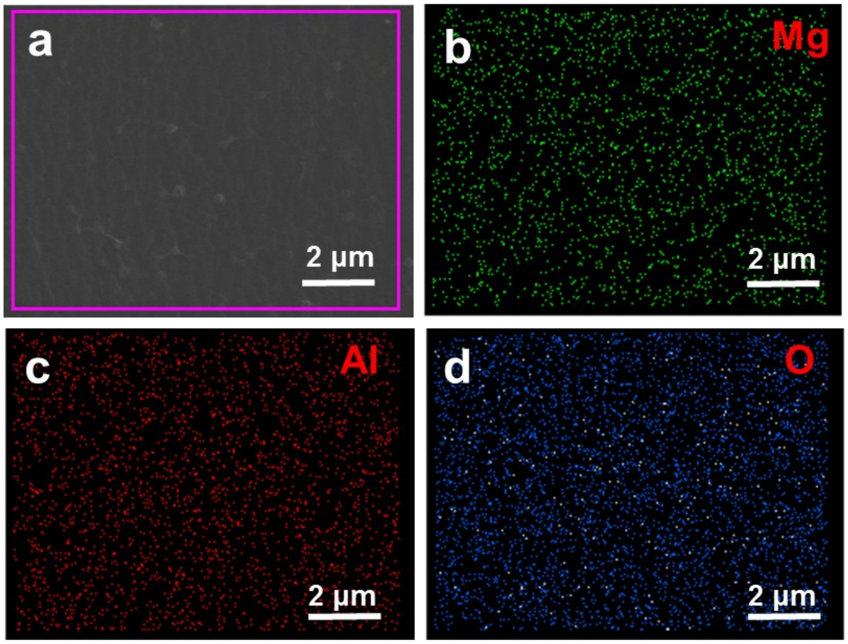

Figure S7. (a) SEM image and (b-d) the EDS mapping results of (LDH/GO)$_{20}$-PP separator.

Figure S8. Photographs of the PDA/PP separators after thermal treatment.

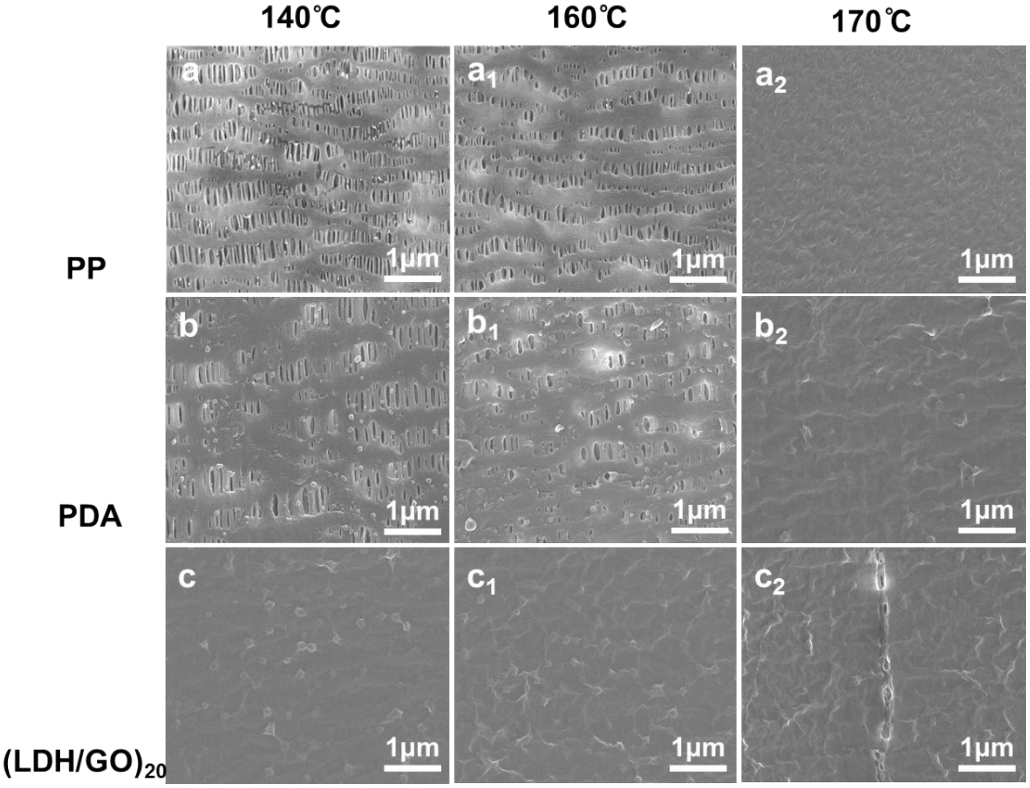

Figure S9. SEM images of (a) PP, (b) PDA/PP and (c) $(LDH/GO)_{20}$-PP separator after heat treatment at different temperatures.

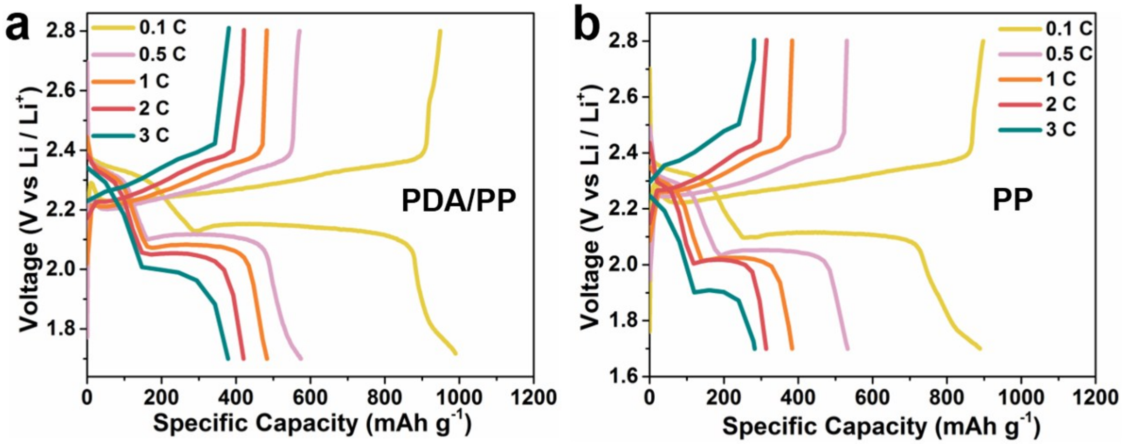

Figure S10. Charge/discharge curves of (a) PDA/PP and (b) PP separators assembled Li–S batteries at various current densities.

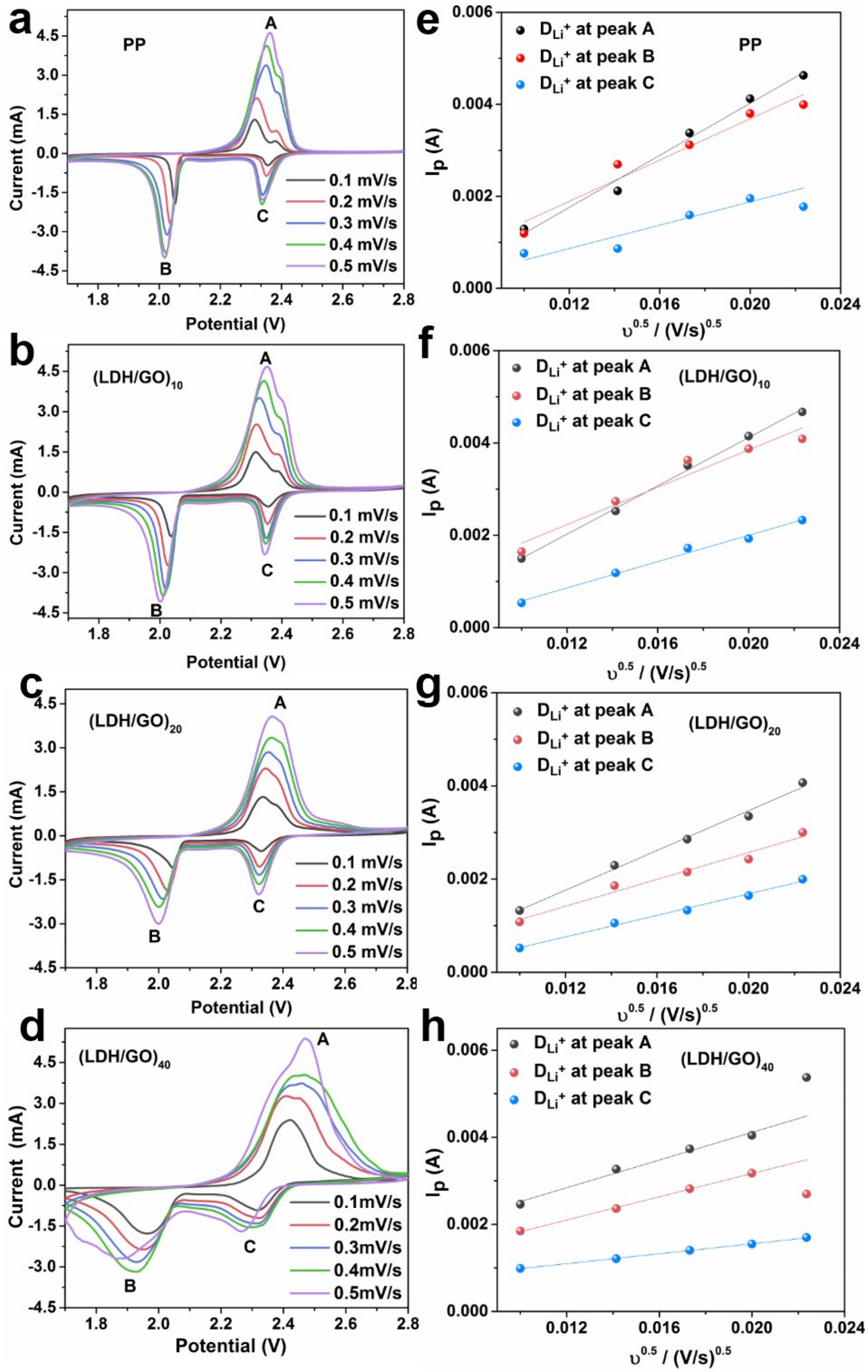

Figure S11. (a-d) CV curves of PP and (LDH/GO)$_n$-assembled Li–S batteries at various scan rates. (e-h) The corresponding linear fitting of the peak currents with the square root of the scan rates for the PP and (LDH/GO)$_n$-assembled Li–S batteries.

Table S1. Summary of Li^+ diffusion coefficients (D_{Li^+}) for different separators

Sample	D_{Li^+} **at peak A** **[cm^2 s^{-1}]**	D_{Li^+} **at peak B** **[cm^2 s^{-1}]**	D_{Li^+} **at peak C** **[cm^2 s^{-1}]**
PP	$2.81*10^{-14}$	$1.83*10^{-14}$	$6.08*10^{-15}$
(LDH/GO)$_{10}$	$2.60*10^{-14}$	$1.57*10^{-14}$	$8.13*10^{-15}$
(LDH/GO)$_{20}$	$2.25*10^{-14}$	$1.34*10^{-14}$	$7.50*10^{-15}$
(LDH/GO)$_{40}$	$9.71*10^{-15}$	$6.92*10^{-15}$	$1.31*10^{-15}$

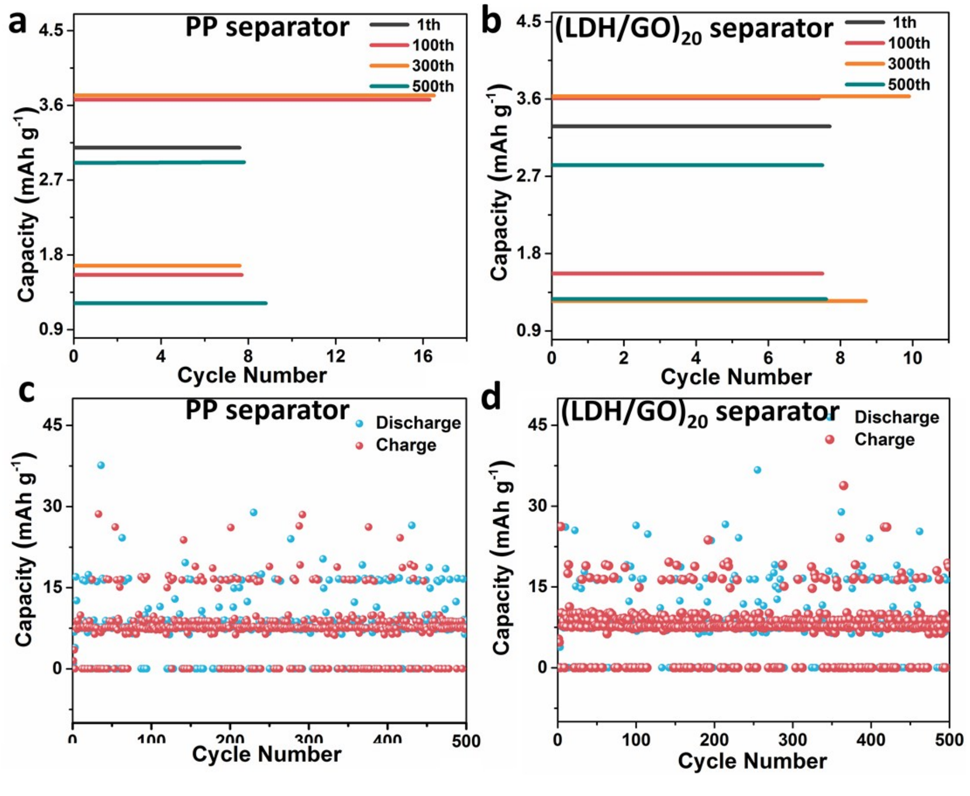

Figure S12. The charge/discharge curves of the batteries with (a) PP and (b) (LDH/GO)$_{20}$-PP separator at different cycle numbers. Cycling performance of (c) PP and (d) (LDH/GO)$_{20}$-assembled sulfur-free batteries.

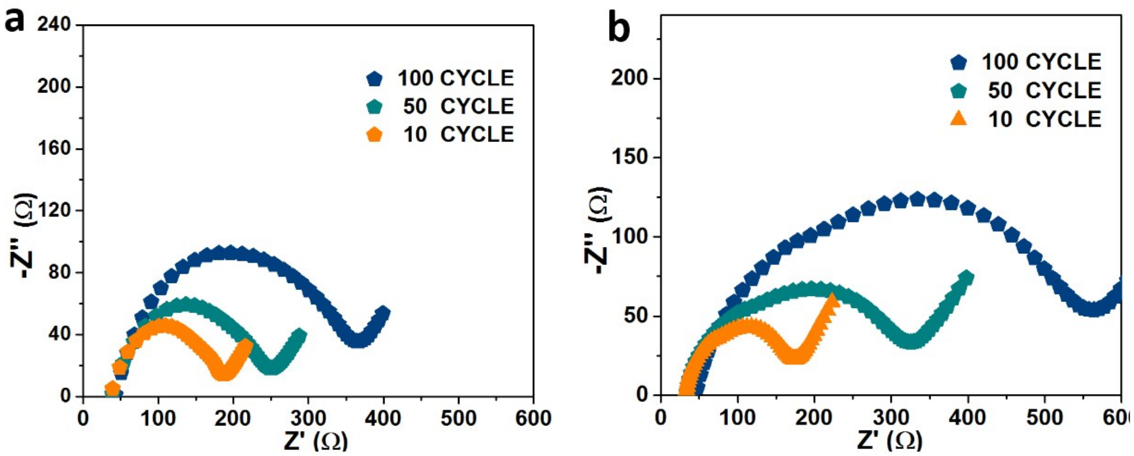

Figure S13. Electrochemical impedance spectra of Li-S batteries with (a) pp and (b) $(LDH/GO)_{20}$-PP separator after different charge/discharge cycles.

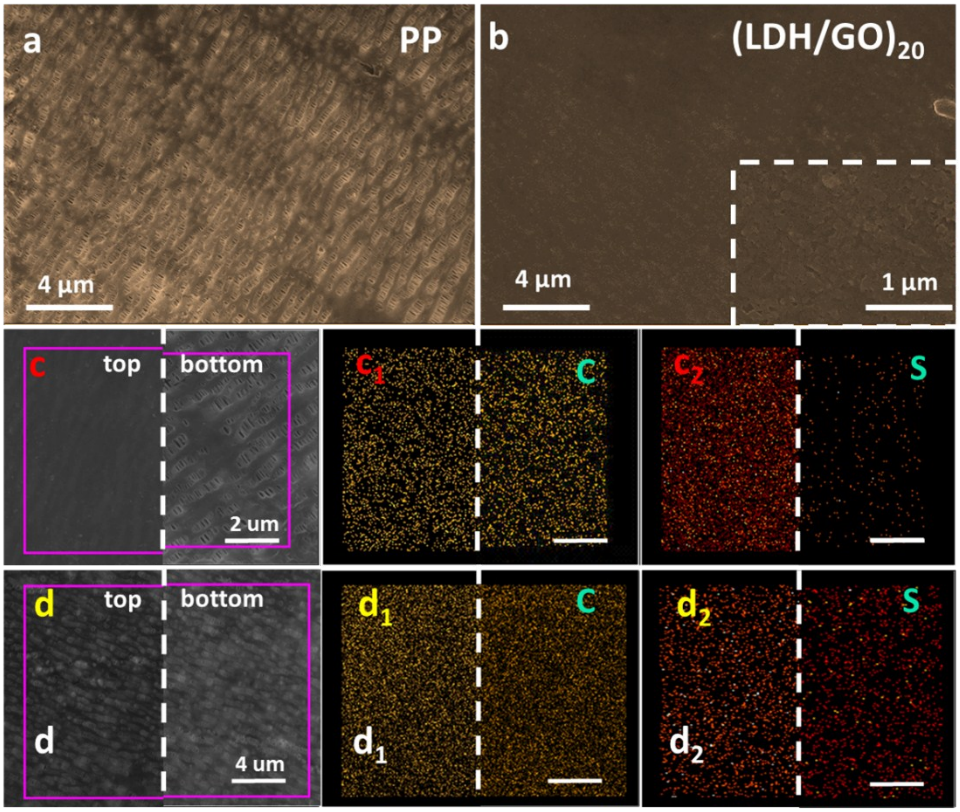

Figure S14. SEM images of (a) PP separator and (b) $(LDH/GO)_{20}$-PP separator (inset: high magnification) after 500 charge/discharge cycles. (c) SEM images and the corresponding EDS mapping results of the both sides of PP separator and $(LDH/GO)_{20}$-PP separator after 500 charge/discharge cycles.

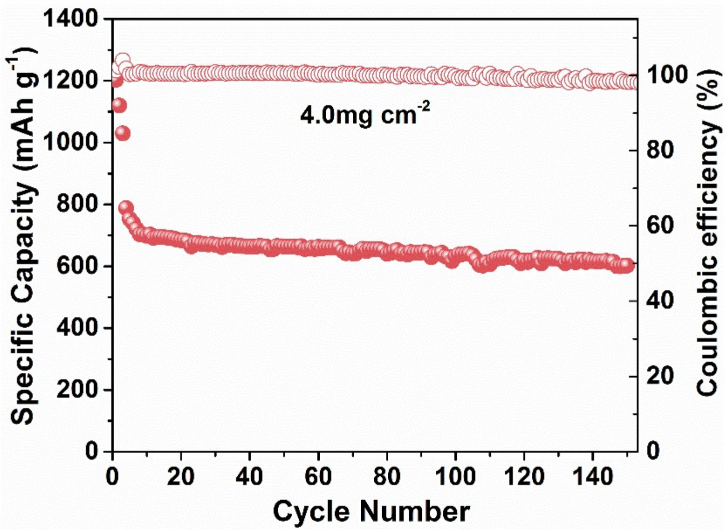

Figure S15. Cycling performance of $(LDH/GO)_{20}$-assembled Li–S battery with high S loading.

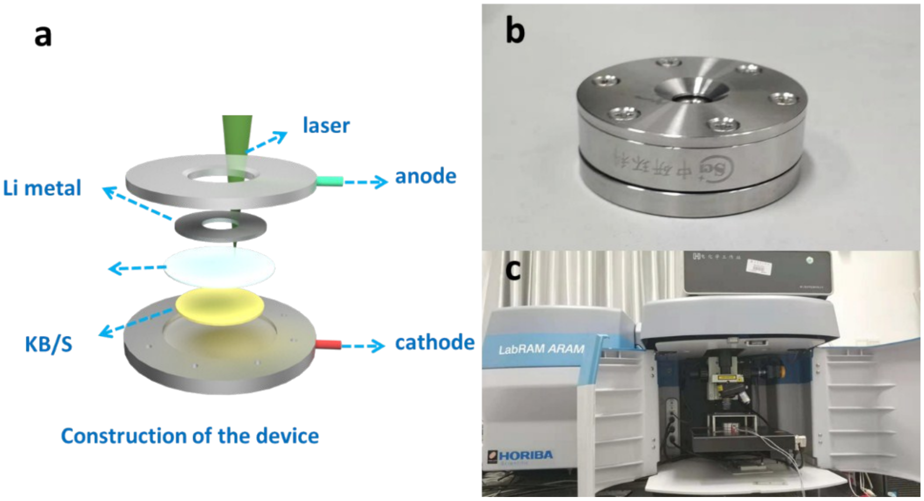

Figure S16. (a) Scheme illustration and (b,c) photograph of the operando Raman device.

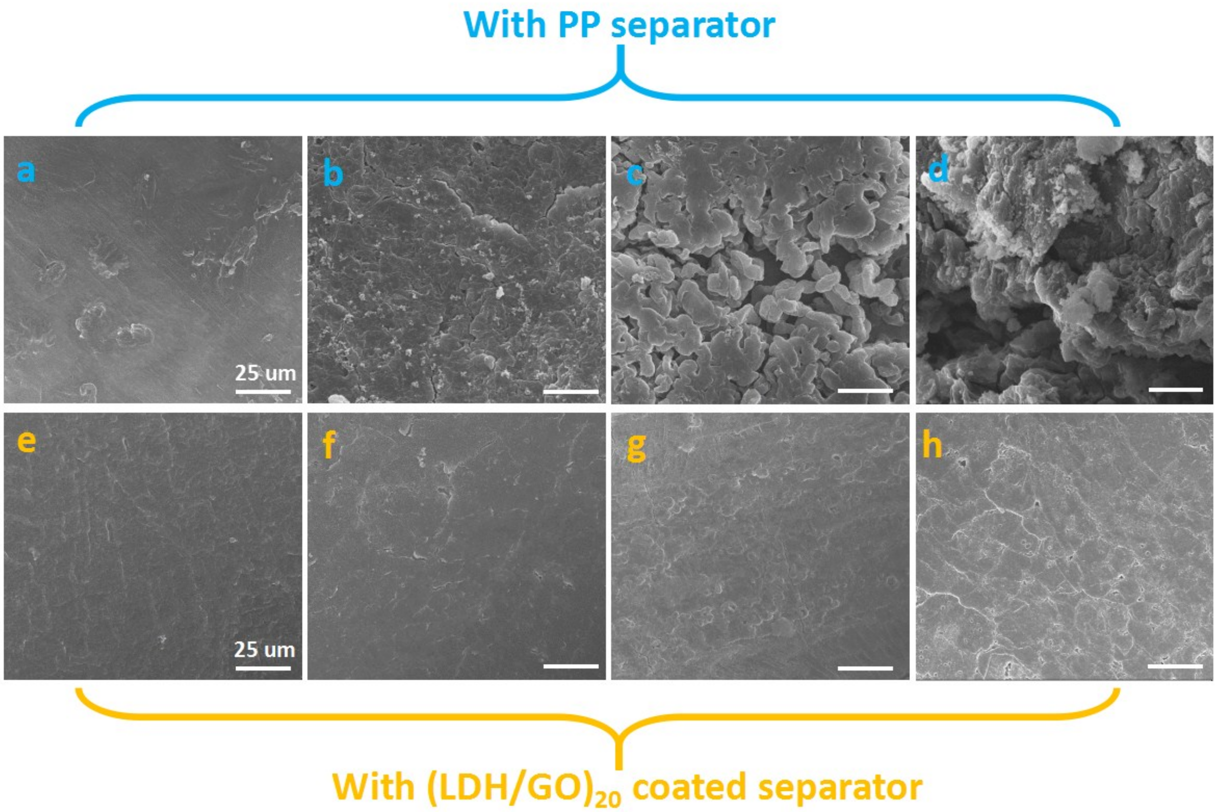

Figure S17. SEM images of the Li metal anode with PP and $(LDH/GO)_{20}$-PP separator after different cycles.

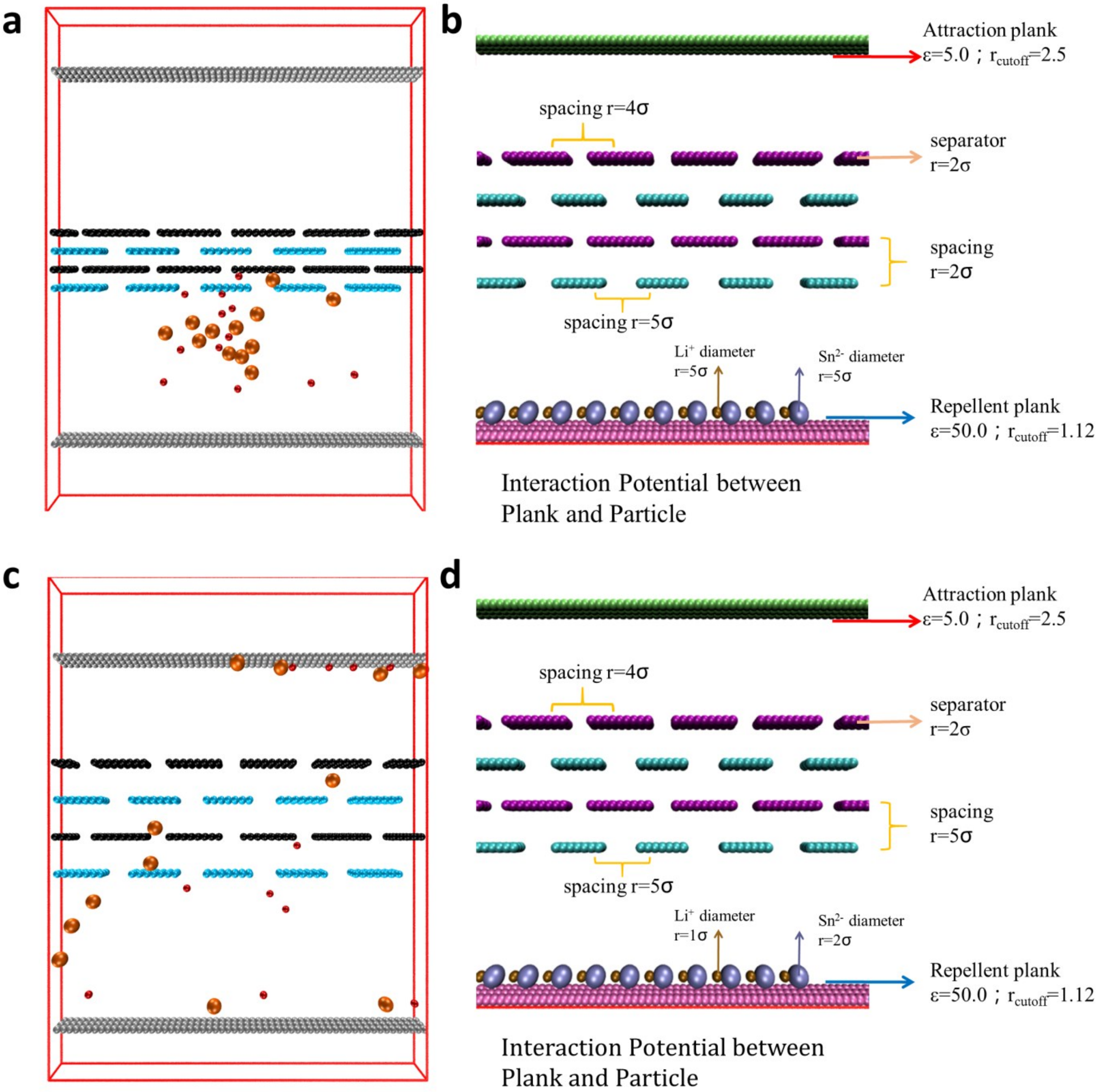

Figure S18. The optimized geometry of LDH/GO LBL models with different interlayer distance.